Distribution Agreement

In presenting this thesis as a partial fulfillment of the requirements for a degree from Emory University, I hereby grant to Emory University and its agents the non-exclusive license to archive, make accessible, and display my thesis in whole or in part in all forms of media, now or hereafter now, including display on the World Wide Web. I understand that I may select some access restrictions as part of the online submission of this thesis. I retain all ownership rights to the copyright of the thesis. I also retain the right to use in future works (such as articles or books) all or part of this thesis.

Shuang Gao April 11, 2017

Computational Fluid Dynamics for Coronary Diseases:

Analysis of Different Murray's Law Based Boundary Conditions

by

Shuang Gao

Alessadro Veneziani
Adviser

Department of Mathematics and Computer Science

Alessadro Veneziani

Adviser

Hao Huang

Committee Member

M Reza Saadein

Committee Member

2017

Computational Fluid Dynamics for Coronary Diseases:

Analysis of Different Murray's Law Based Boundary Conditions

By

Shuang Gao

Alessadro Veneziani

Adviser

An abstract of
a thesis submitted to the Faculty of Emory College of Arts and Sciences
of Emory University in partial fulfillment
of the requirements of the degree of
Bachelor of Sciences with Honors

Department of Mathematics and Computer Science

2017

Abstract

Computational Fluid Dynamics for Coronary Diseases: Analysis of Different Murray's Law Based Boundary Conditions
By Shuang Gao

Coronary Disease is becoming the one of the most serious threat toward human health. In most cases, atherosclerosis is responsible for the coronary artery stenosis, which further leads to coronary diseases. Investigating the abnormal blood flow pattern in coronary artery provides a way to inspect the existence of coronary artery stenosis. In this paper, we will first study the use of Murray's law in computational fluid dynamics and specify how to construct the Murray's law based boundary condition.

Further, we will introduce the general form of Navier-Stokes equation, which offers a mathematical model for fluid flow and related phenomena. In this research, the blood flow is our main interest. Several simplifications on Navier-Stokes equation allow us to depict blood flow in the vessel properly. Such modification leaves us the steady three-dimensional Navier-Stokes equation for incompressible Newtonian viscous fluid. The weak formulation of the modified Navier-Stokes equation is then introduced, which will be utilized in the computational fluid dynamic procedure to approximate the solution. In order to solve the Navier-Stokes equation with FreeFem++, the finite element method is chosen for space discretization and Picard iteration scheme is selected to linearize the problem. The previous steps together provide the algorithm to solve for the pressure and velocity of blood.

With the solutions of Navier-Stokes equations with different Murray's law based boundary conditions, we calculated and compared the pressure drop and flow split. The results showed the choosing exponent between 2.25 to 2.75 in Murray's law will not significantly affect the Navier-Stokes solutions.

Computational Fluid Dynamics for Coronary Diseases:

Analysis of Different Murray's Law Based Boundary Conditions

By

Shuang Gao

Alessadro Veneziani

Adviser

A thesis submitted to the Faculty of Emory College of Arts and Sciences
of Emory University in partial fulfillment
of the requirements of the degree of
Bachelor of Sciences with Honors

Department of Mathematics and Computer Science

2017

Acknowledgements

I would like to acknowledge Dr. Alessadro Veneziani for his help and guidance on this research project. I would like to thank Alex Viguerie, who took the role of co-advisor and gave me great support on programming. I would also like to thank Dr.Hao Huang and Dr. M Reza Saadein for their patience and encouragement. Finally, I am grateful to my parents, who have shaped me who I am today.

Table of Contents

List of Figures

List of Tables

Chapter 1

Introduction

1.1 Coronary Arteries Disease

The Cardiovascular system is an essential component of the human body, which guarantees all the physiological processes functioning properly. In the cardiovascular system, there are two fundamental constituents: the heart and blood vessels (aorta, arteries, arterioles, capillaries, venules, veins, venae cavae)[1]. The human heart, the pump of the cardiovascular, pushes blood to flow through aortas and carries nutrients including oxygen to every cell in human body. In this process, each organ receives enough supplements to keep physiological activities functioning at a normal level. The deoxygenated blood then goes back from peripheral capillaries to the heart through the veins. The muscle pump, a vital part of blood circulation, generates the force to contract surrounding muscles. Such skeletal-muscle pump action, happening during breathing, facilitates the return of venous blood to the heart [2].

Aorta, as the main blood carrier in a human body, originates from the left ventricle of the heart [3]. It then splits into two daughter branches: the left coronary artery and the right coronary artery. The right coronary artery brings blood volume to the right portion of the heart. The left coronary artery carries blood supply to the left side of the heart. Both of these two main coronary blood vessels reside on the surface of the heart and then branch off into smaller arteries, supplying blood output to every tissue and organ in the human body [1, 4].

Coronary Arteries Disease, mostly appearing with the chest pain and symptoms consistent with myocardial ischemia, is responsible for about 8% to 10% of the 119 million Emergency Department visits every year [7]. According to the data from World Health Organization, "coronary artery disease was responsible for 7.2 million deaths, or 12.2% of all deaths globally and 5.8% of all years of life lost. The disease is highly prevalent: at any given time, 54 million people in the world suffer from angina pectoris and 23.2 million people experience moderate to severe disability as a result of ischemic heart disease "[8]. As the modern society develops rapidly, people have to adapt to fast-pace lives, which results in unhealthy life style, such as smoking and excessive alcohol. As the outcome of these harmful habits, hypertension, hyperlipidemia, obesity and high blood cholesterol symptoms occur and raise the cardiovascular risk [9].

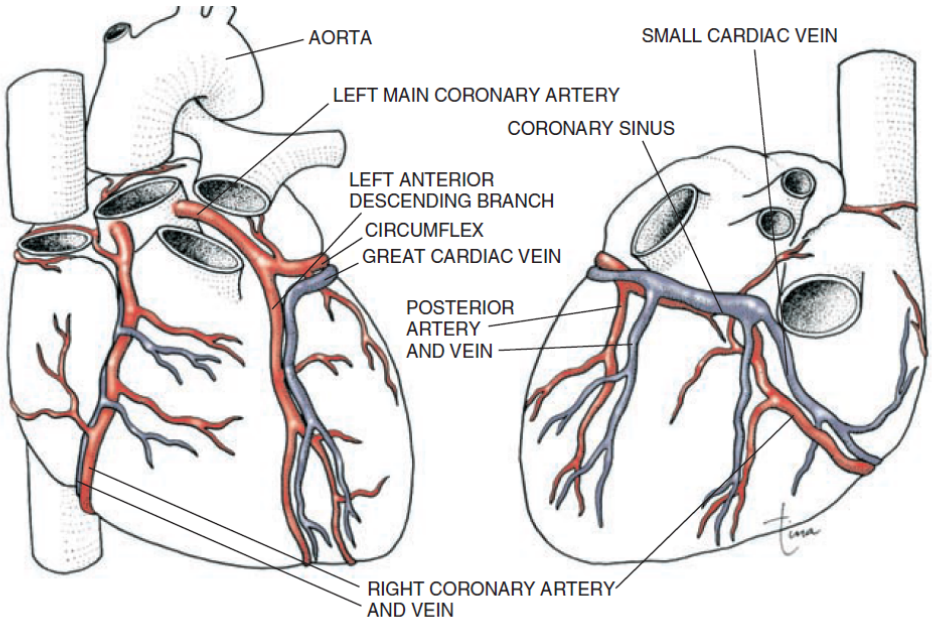

Figure 1.1 Illustration of aorta branches in human heart [1]

However, Coronary Arteries Disease is not only prevalent and recognized in recent years. Tracing back to 18th century, the symptom of atherosclerosis was first recognized and then

recorded by the Italian anatomist Giovanni Morgani [10]. A few years later, the British physicians, Edward Jenner and Caleb Parry, realized the connection between the disorder of the breast and atherosclerosis described by Giovanni Morgagni [10]. As more and more people suffered from the sudden cardiac death, doctors and physicians shifted their focus onto the pathological cause of these demises. Until 20th century, the American doctor, James Herrick, proposed that "thrombotic occlusion of the coronary arteries plays a central role in myocardial infarction", and built the pathophysiological foundation of coronary artery disease [10]. As the first one to offer pathological explanation of real patients' symptoms, Herrick undoubtedly lead later scientists to discover the unknowns of coronary arteries diseases.

A common symptom of coronary arteries disease is chest pain. Several seconds of chest pain may not be considered as a sign of serious heart disease. However, the underlying pathology of this acute cardiac disorder is "cute intraluminal coronary thrombus formation within an epicardial coronary artery leading to total or near total acute coronary occlusion" [5]. If human organs function normally, the blood supply along with nutrients will be pumped out from the heart and to the rest of the body to maintain physiology. Nevertheless, when heart muscle cannot generate enough force to push blood volume out or other cases, the terminal parts of the human body will not receive sufficient amount of supplement to complete their own tasks. As a result, physical functions of organs and systems decline, which later cause the sudden cardiac death.

As the carrier of blood supply, arteries act a crucial role of passing supplement from heart to the rest part of a body. To be specific, the two main coronary arteries, the （two daughter branches of aorta）have the responsibility of delivering blood to the myocardium (heart muscle). Nevertheless, sometimes abnormal situations occur, such as hardening or clogging of the blood

vessels. In these cases, the coronary arteries begin to narrow down or be blocked by the blood clot. The narrowed coronary arteries lose their abilities to alter the blood flow and pressure properly and cannot supply adequate blood along with oxygen and nutrients to the myocardium. Then the heart does not have enough energy to control the muscle pump action, which results in the occurrence of heart attack or angina [11]. The coronary artery disease, caused by the coronary arteries stenosis, is the leading cause of death in industrialized society. In the U.S., coronary artery disease accounts for one-sixth of total death in 2010 [12]. As the etiology of coronary artery disease, the narrowing or the blockage of the coronary arteries are usually caused by atherosclerosis [11].

1.2 Atherosclerosis

Nowadays, people suffered from serious coronary arteries diseases caused by atherosclerosis and have no effective treatment to cure the morbidity. Although atherosclerosis has been recognized for a long time, the discoveries of the pathological mechanism are not complete [13].

Atherosclerosis is the accumulation of cholesterol and fat on the arterial walls and therefore is the syndrome that affecting the blood vessel conditions [11]. As the white blood cells and fibrofatty plaque accumulate on the inner surface of blood vessels, the coronary arteries walls thicken and the blood supplying path is blocked [13]. In normal cases, coronary arteries are smooth and elastic vessels, which allow blood flow through. On the surface of inner wall of coronary arteries, the layer of cells called endothelium separate blood flow from the arterial surface. The endothelium also releases chemical signals, in order to give responses to different stimuli. In this way, the endothelium assists to regulate the artery functions [13]. With the

elasticity and the help of endothelium, coronary arteries can adapt themselves to different blood pressure and guarantee the blood supply to the heart. However, as the fibrofatty in the blood flow passing by, they addict to the inner arterial wall. With the other substances, such as cholesterol, all the substances gather to form plaque. After atherosclerosis occurs, the plaque on the inner surface may lead to the formation of blood clots and then block the coronary arteries. The abnormality of endothelium reaction can also make the artery squeeze improperly, which account for the coronary arteries stenosis. Due to atherosclerosis, the arteries become rigid and narrowed, and cannot response to blood pressure changes appropriately. The coronary arteries obstruction limits blood flow passing through the arteries to the heart. Lacking adequate nutrients, the heart muscles do not function normally and finally get injured, inducing sudden cardiac death [14].

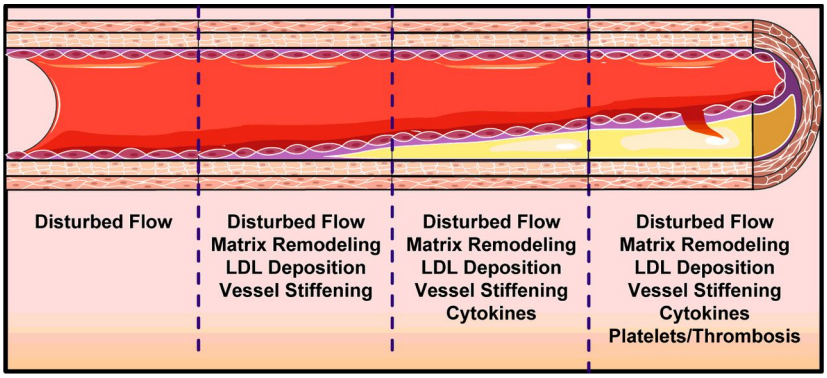

Figure 1.2 Accumulation of fibrofatty results in coronary artery stenosis [26]

1.3 Computational Fluid Dynamics

In the twentieth century, the invention of digital computers boosted the development of computing, as people solved for numerical solutions by powerful computer instead of by hands [15]. Such change incredibly speeded up computation process, limited calculation error made by

hands and allowed operating a lot of calculations at the same time. The good performance of computers prompted the development of computational fluid dynamics.

Fluid is the smallest molecule structure, which will be deformed by any force. Such structure “offers no resistance to external shear forces” [16]. When any external force is applied to fluids, the fluid flow forms. In the common approach, the simplified equations of fluid dynamics are solved with approximation and dimensional analysis, where empirical data is needed. However, for some flows (air around aircraft etc.), the dimensionless parameters are required. In these cases, experiments are not helpful to give the scales of the actual flow [16]. With the help of the computer, the field of computational fluid dynamics developed and became the alternatives to experiments, in order to provide the numerical analysis of fluid flows. CFD provides the prediction and qualitative analysis by solving the partial differential equations describing fluid flows.

CFD methodology is implemented in the following procedures:

1. Mathematical model: choose an appropriate model for the stated problem. Make sure the conservation law of matter, momentum, and energy is satisfied. Include plausible assumptions to the equations used in the model, in order to reduce the computational effort. Impose boundary and initial conditions to the model.

2. Discretization: for the given geometry, discretize the domain and generate the mesh with proper polynomials, in order to approximate the differential equations by a system of algebraic equations [16]. There are many useful discretization methods, such as finite difference, finite volume, and finite element methods.

3. Iteration scheme: For the system of algebraic equations yielded by discretization, choose the proper iteration scheme to solve for the solution. The iteration process stops when the convergence criteria are satisfied.

4. Post-processing: extract the targeted information from the computed fluid field. Visualize the simulation results with graph.

Compared to the experimental approach to fluid dynamics, using computer simulations in CFD field provides complimentary advantages:

1. Physical models can be only generated at a laboratory scale. For some unrealistic conditions, it is impossible to solve for the solutions of simplified mathematical models. However, for CFD, the realistic conditions can be imposed to the model. The computer simulations will replicate the extreme requirements and provide the numerical solutions. This indicates the CFD approach can be used for more cases.

2. Restricted to the precisions of laboratory instruments, experiments provide the solutions at a limited number of space positions and restrictive time points. CFD approach with high resolution is able to solve for solutions at more points in space and time.

3. The efficiency of experiments depends on the complexity of fluid flow models. In common conditions, it is expensive to conduct experiments. The experimental results may take a long time to achieve. The alternative CFD approach generates the mesh and runs simulations on a computer. The efficiency depends on the computing ability of computers. As the technology advances rapidly, the computing cost is relatively low and simulation process takes less time, compared to conducting experiments.

Despite the advantages, CFD technique has, simulation results are not always reliable. The numerical errors may come from each step of CFD approach. The approximation in the discretization step accounts for the truncation error. The round-off error depends on the computing ability of the machine. The accuracy of the solutions needs to be stressed. The results may be sensitive to the input boundary conditions.

CFD methodologies are implemented in biology, astrophysics, meteorology and other fields [17]. The relatively low cost and fast speed of simulation attract engineers' interest and enable them to perform numerical experiments. The large demand for CFD application leads to the development of simulating software, such as FreeFem++, Fluent, and FemLab.

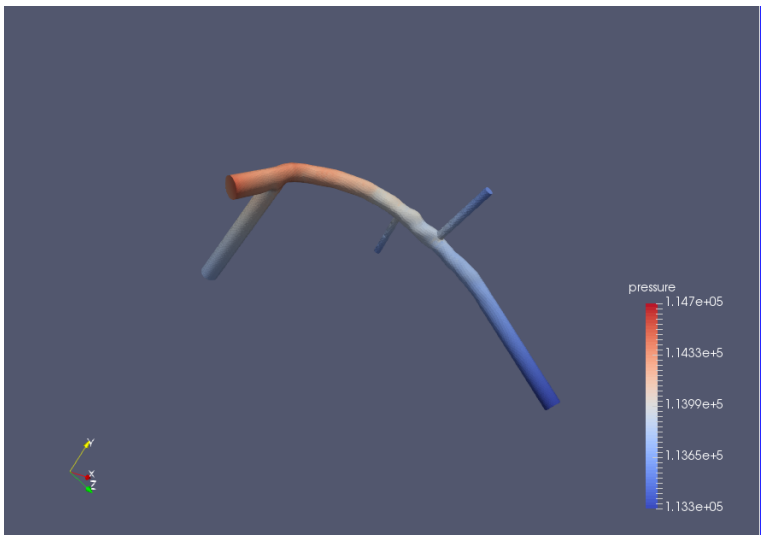

Figure 1.3 Pressure result of the three-branch geometry simulation viewed by Paraview

1.4 Previous Study

Nowadays, coronary artery disease seriously threatens the health of people worldwide, accounting for hundreds of thousands of death each year [5]. The coronary artery disease is caused by the coronary artery stenosis, which is usually resulted by atherosclerosis. There is a study conducted to examine the relation between vessel wall shear stress and the rate of

atherosclerosis progression, which clearly indicates the existence of the connection between atherosclerosis and blood flow patterns [18]. From the previous section, the fluid flow can be analyzed by computational fluid dynamics approach, in order to further discover the knowledge of atherosclerosis.

In the study conducted by Doutel, they focused on the application of Murray's law on bifurcation cases and utilized CFD methodology in a real case to indicate the power of including Murray's law into the numerical analysis of fluid dynamics. They took Murray's law as a reference and studied the left coronary artery bifurcation by numerical simulation. They designed the idealized left coronary artery geometry with the average value of human left coronary artery data. Because Murray's law gives the relation between the radius of parent branch and radius of its daughter branches. More restrictions were required for the size of the vessel geometry. Murray's law also gives the restriction on the allocation of the flow rate in the branches, which are significant for constructing boundary conditions. In Doutel's study, they also set the angles between the branches with the reference to Murray's relation. After the blood properties were included, the Navier-Stokes equations for the 3D incompressible flow was constructed. Then the boundary conditions of inlet, wall, and outlet were imposed on the chosen model. The CFD scheme was implemented to solve Navier-stokes equations for various surface area of the outflow branches with the same inlet diameter and same inlet wall shear stress.

The various radiuses of outlet and angles between branches were considered in the configurations of the left coronary artery. The results indicated that geometries constructed according to Murray's law "minimize the energy cost and keep the blood flow in circulation" [19]. This study concluded that for the numerical analysis in bifurcations, Murray's law should be referenced in the geometry construction and flow allocation process. Also, the exponent in

Murray's law is adjusted to be in the range of 2 to 3, in order to deal with real arteries, which do not follow the original Murray's law [19].

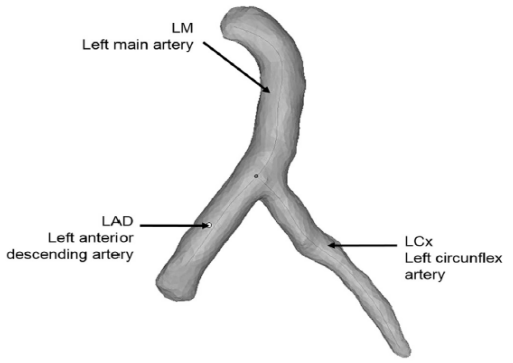

Fig. 1. Schematic representation of the Left Coronary Artery (LCA) near the main bifurcation, including the Left Main Stem (LM), the Left Anterior Descending Artery (LAD) and the Left Circumflex Artery (LCx).

Figure 1.4 The designed LAD geometry in study [19]

1.5 Objective and significance

The blood flow through vessels in a human body is governed by physical laws, in order to fulfill the physiological requirements [21]. For the circulation system in the organism, the branching vasculature assists to supply blood volume to every organ, in order to transport the oxygen and nutrients. As the bifurcation appears in the vessel structure, the blood flow divides into branches naturally. By analyzing the branching system, Cecil D. Murray realized that "physiological vascular systems, subjected through evolution to natural selection, must have achieved an optimum arrangement such that in every segment of vessel flow is achieved with the least possible biological work" [21]. From Murray's study, in the numerical analysis of the allocation of blood flow in branches, energy minimization principles need to be considered. As the result, Murray's law was introduced, which gave the relation between radius of a parent vessel and radii of the daughter branches by the following formula,

$$R_{in}{}^{p} = R_1{}^{p} + R_2{}^{p} + \cdots + R_n{}^{p} \tag{1.1}$$

Where R_{in} is the radius of parent vessel, and $R_1, R_2, R_3 \ldots R_n$ are the radii of the respective daughter branches [20].

A large amount of branching system obeys Murray's law. The validity of Murray's law guarantees its application into the various study. For instance, Murray's law is regarded as a biomimetic design tool in engineering and also utilized in research on vascular network changes in the retina [20, 22]. In the previous section, Doutel's study also indicated the power of Murray's law in fluid dynamics. This study demonstrated the reference to Murray's law provided additional information for boundary conditions and vessel geometry generation, and the exponent in Murray's law could be adjusted in the range of 2 to 3. Although the study conducted by Doutel discussed the use of Murray's law in bifurcation cases, it did not clearly state how sensitive the flow pattern result is to the chosen exponent in Murray's law.

The objective of this research is to further study the application of Murray's law in human coronary artery. Different values of the exponent (between 2 and 3) in Murray's law will be considered into the research. The geometry of coronary artery with three branches will be utilized for each case. The steady Navier-Stokes equation is selected as the mathematical model of the flow pattern in the chosen geometry. With the help of FreeFem++, the blood velocity field and pressure results will be simulated numerically with the CFD approach. It is hypothesized that the change of exponent in Murray's law will affect the flow in the coronary arteries. The results of pressure drop and flow split will be examined in Matlab. The comparisons between each case with a different exponent in Murray's law will be analyzed, which lead to the conclusion of the impact of changing the exponent.

The pressure field results help to measure the pressure difference in the branches of the coronary arteries. Such information is required for calculating the fractional flow reserve, which is a technique used to study the influence of the coronary artery stenosis on pressure change [23]. This research of the impact of changing exponent on blood flow pattern gives the guideline on selecting the proper parameter for Murray's law. As a result, the method of allocating blood flow in branches based on Murray's law will not greatly arouse the change in fluid velocity and pressure field. In this way, physicians can achieve a better result of fractional flow reserve, which will give them some insights on the study and coronary arteries disease.

Chapter 2

Methods

In this section, the chosen geometry and flow profile will be introduced. The three-dimensional Navier-Stokes equations stemming from conservation of mass and momentum are selected for the mathematical model of the blood flow. A set of boundary conditions is imposed on the mathematical model. A detailed description of the numerical simulations will be included.

2. 1 Data

2.1.1 Geometry

In order to study the exponent changes in Murray's law, a geometry with bifurcation is needed for this research. From a real patient, we get the coronary artery data to form the three-dimensional structure of blood vessel. To focus on the allocation ratio of blood supply in the coronary artery, the blood vessel with three daughter branches is chosen for the study. The data of the geometry is retrieved from a clinical study on real patients. The geometry is reconstructed from images with vascular modeling toolkit.

For the upcoming analysis with finite element method, which will be introduced in later session, the mesh of the given geometry needs to be generated. For such step, the automatic mesh generator, Netgen, is utilized. It can generate mesh for solid geometry or boundary representation. It can also label the sub boundary in the given figure. Both two and three dimensional surface meshing and three dimensional volume meshing are allowed in Netgen [24]. This software can efficiently generate mesh for later computational fluid dynamics study.

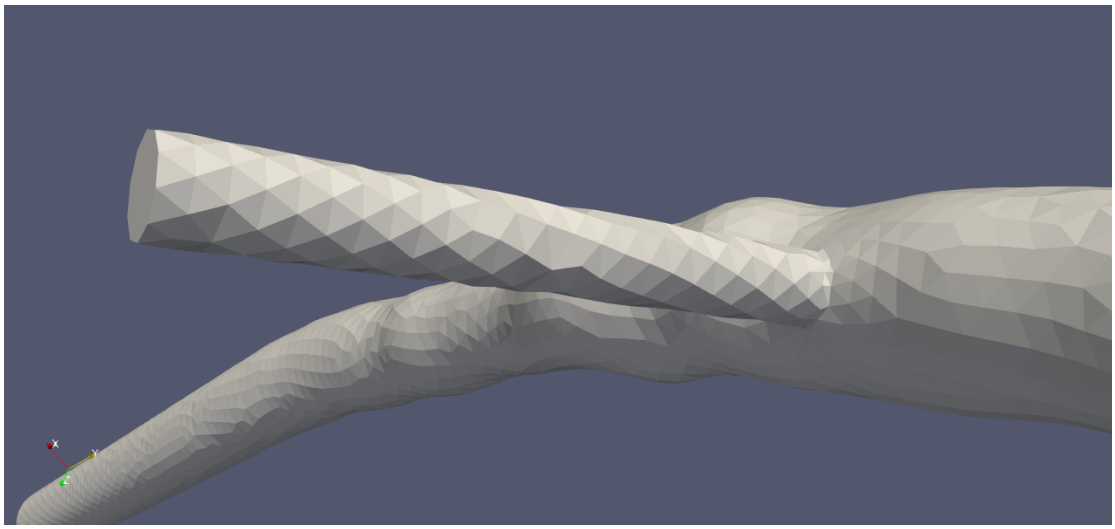

Figure 2.1 The mesh generated for specific 3D structure with Netgen

For the chosen geometry in Figure 2.1, Netgen is used to create a fine mesh. As a result, 7466 vertices, 13074 triangles, and 35026 elements are created for the structure.

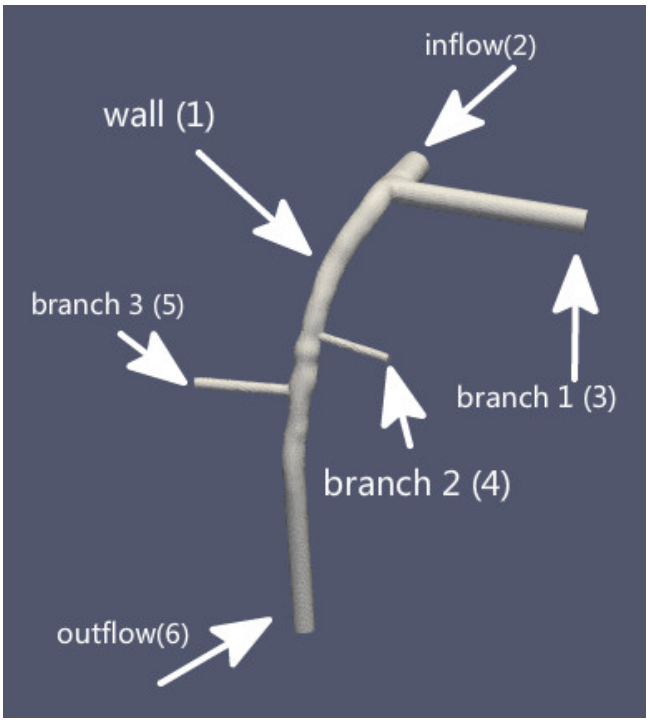

Figure 2.2 The label of surface in the geometry for later study on boundary conditions: *(1) inflow labeled as 2 (2) wall labeled as 1 (3) branch 1 labeled as 3 (4) branch 2 labeled as 4 (5) branch 3 labeled as 5 (6) outflow labeled as 6*

For the later study on boundary conditions, the surfaces of the coronary artery structure need to be labeled in a certain sequence. We label the whole wall of the vessel as region 1, label the inflow as region 2, and label the three branches respectively as 3, 4 and 5, and finally, label the outflow as 6. All the labels and blood flow are introduced in Figure 2.2.

2.1.2 Boundary Conditions

For specific mathematical model, the boundary conditions of the blood flow on the given domain are required to give more information for the differential equation. In this research, the use of Murray's law imposes the energy minimization principle for the blood supply in the coronary artery branches. In this manner, the flow rate in each branch will be calculated by the following formula:

$$Q_i = \left(\frac{r_i}{r_{in}}\right)^p * Q_{in} \tag{2.1}$$

where Q_{in} is the given flux of the inlet, r_{in} is the radius of the parent branch, r_i is the radius of the daughter branches, Q_i is the flux flowing in the corresponding branch and p is the exponent in Murray's law. In order to study the impact of changing exponent in Murray's law, we let p to be 3.00, 2.75, 2.50 and 2.25 respectively and analyze the pressure changes in each branch in the following sections.

The selected geometry of coronary artery with three branches is a three-dimensional structure. Thus, the blood flow in the vessels also needs to be interpreted in the three-dimensional space. In order to set up the boundary conditions for the inflows and outflows, we need to construct the flow profile for the blood flowing through according to the blood characteristics.

For fluid, one property we need to consider is the viscosity, which means its resistance to the deformation of the structure by shear stress [25]. In this research, we assume that the velocity of blood flow in this study will achieve its maximum at the center of the vessel and have zero value on the boundary. As a result, the blood flow in the coronary artery can be characterized by laminar flow, which depicted by concentric layers moving parallel to the vessel wall. To consider the velocity **u** as a function of position **x**, the velocity will have the largest value at the center of the vessel and reach the lowest value at the edges. Thus, the parabolic profile function is introduced to depict the blood flow in the vessels. However, the center of mass needs to take into account for the center shift of the blood flow. From the FreeFem++, the center of mass along three perpendicular axis is measured asM_x, M_y and M_z for each boundary. Then the parabolic profile of the blood flow is characterized by the following function,

$$f(x,y,z) = 2 * \left(1 - \frac{(x-M_x)^2+\left(y-M_y\right)^2+(z-M_z)^2}{r^2}\right) * \frac{1}{A} \tag{2.2}$$

where r is the radius of the branch, A is the area of the boundary surface. This formula gives the parabolic profile of blood and helps to investigate the boundary conditions needed for the mathematical model.

With the parabolic function of blood flow and the calculated flux at the boundary of each branch, this research focuses on five different cases, varying in boundary conditions or exponent in Murray's law. To be specific, the five cases are stated as below.

Case 1: blood flow model with traction free conditions at the outflow (roughly corresponding to zero pressure) and exponent = 3.00 for the collateral vessels

Case 2: blood flow model with Dirichlet boundary condition and exponent = 3.00

Case 3: blood flow model with Dirichlet boundary condition and exponent = 2.75

Case 4: blood flow model with Dirichlet boundary condition and exponent = 2.50

Case 5: blood flow model with Dirichlet boundary condition and exponent = 2.25

The comparison between the first two cases aims at investigating the significance of imposing boundary conditions to the model. The comparison between the last four cases aims at investigating the impact of changing the exponents in Murray's law.

2.2 Mathematical Model

2.2.1 Navier-Stokes equation

Fluid dynamics is the area where the motion of fluid particles gains the great interest of scientists. In the microscopic level, fluid is a series of infinitesimally small molecules. When the density of the fluid is very large, we can regard the fluid as a continuum. In this manner, we can investigate the pressure, velocity and other properties at each point [27]. To study the behavior of the fluid, the system of Navier-Stokes equations is introduced. With the conservation of momentum, mass, and energy, the Navier-Stoke equation describes the motion of the fluid and related flow phenomena. The general form of Navier-Stokes equation describing a viscous, incompressible Newtonian fluid in a bounded domain $\Omega \subset \mathbb{R}^3$ is shown as follow:

$$\begin{cases} \frac{\mathbf{u}}{\mathrm{t}} - v\Delta\mathbf{u} + (\boldsymbol{u}\cdot\nabla)\boldsymbol{u} + \nabla p = \boldsymbol{f} & in\ \Omega\times(0,T] \\ \nabla\cdot\mathbf{u} = 0 & in\ \Omega\times(0,T] \end{cases} \tag{2.3}$$

Where **u** is the fluid velocity, p is the pressure divided by density, **f** is the forcing term, ρ is the density of the fluid, μ is the dynamic viscosity, and $v = \frac{\mu}{\rho}$ is the kinematic viscosity. The first equation in (2.3) is derived from the conservation of linear momentum. The second equation

in (2.3) comes represents the incompressibility condition. $\frac{\mathbf{u}}{\mathrm{t}}$ term indicates that the fluid is unsteady, which means the fluid changes with time. $v\Delta\mathbf{u}$ is the diffusion term, which describes how fluid is damped. $(\boldsymbol{u}\cdot\nabla)\boldsymbol{u}$ is the nonlinear transport term. Together with the appropriate initial condition and boundary conditions, the system of Navier-Stokes equation forms.

Blood, which takes 8% body weights, is composed of blood cells and plasma [28]. As a complex mixture, blood is not homogeneous and thus cannot be considered as Newtonian fluid. However, the blood plasma is a Newtonian fluid, because most of its composition is water [29]. Also, it is hard to model the non-Newtonian fluid, due to its complexity. Thus, we assumes that blood in large vessel is considered as a Newtonian fluid. We also make the assumption that the blood flow in coronary artery does not change with time, which means the blood flow is steady. To further simplify the problem, we take the forcing term as zero. Such assumptions lead the choice of three-dimensional Navier-Stokes equations and continuity equation for incompressible Newtonian viscous fluid. Thus, the equations in (2.3) changes into the following form,

$$\begin{cases} -v\Delta\mathbf{u} + (\boldsymbol{u}\cdot\nabla)\boldsymbol{u} + \nabla p = \mathbf{0} & in\ \Omega \\ \nabla\cdot\mathbf{u} = 0 & in\ \Omega \end{cases} \tag{2.4}$$

where **u** is the fluid velocity, p is the pressure divided by density, ρ is the density of the fluid, μ is the dynamic viscosity, and $v = \frac{\mu}{\rho}$ is the kinematic viscosity. The domain Ω is defined as the geometry in Figure 2.2 and $\partial\Omega = \Gamma_1 \cup \Gamma_2 \cup \Gamma_3 \cup \Gamma_4 \cup \Gamma_5 \cup \Gamma_6$ (regions are labeled in Figure 2.2). The Dirichlet boundary conditions are shown as below,

$$\begin{cases} \boldsymbol{u} = \mathbf{0} & \forall \boldsymbol{x} \in \Gamma_1 \\ \boldsymbol{u}(\boldsymbol{x}) = Q_{in} f \boldsymbol{n} & \forall \boldsymbol{x} \in \Gamma_2 \\ \boldsymbol{u}(\boldsymbol{x}) = Q_3 f \boldsymbol{n} & \forall \boldsymbol{x} \in \Gamma_3 \\ \boldsymbol{u}(\boldsymbol{x}) = Q_4 f \boldsymbol{n} & \forall \boldsymbol{x} \in \Gamma_4 \\ \boldsymbol{u}(\boldsymbol{x}) = Q_5 f \boldsymbol{n} & \forall \boldsymbol{x} \in \Gamma_5 \\ \boldsymbol{u}(\boldsymbol{x}) = Q_6 f \boldsymbol{n} & \forall \boldsymbol{x} \in \Gamma_6 \end{cases} \tag{2.5}$$

where Q_{in} is the inlet, Q_3, Q_4, and Q_5 are the flux in the corresponding side branches, Q_6 is the outlet, and f is the parabolic profile of blood flow given in equation (2.2).

Another Neumann boundary condition for pressure takes into account. The first derivative of pressure in outflow equals to the given distal pressure. However, this Neumann boundary condition is only utilized for case 2 to 6. Because in case 1, there is no Dirichlet condition for velocity. Thus imposing the pressure condition to this case will lead to the reallocation of the flux, in order to fulfill the conservation law. As a result, the solution with no physical meaning, such as positive flux for outflowing branches, appears.

2.2.2 Weak formulation

First weak formulation of equation (2.4) needs to be derived for later use in finite element method. We start by multiplying the first equation in (2.4) by the test function v and multiplying the second continuity equation in (2.4) by the test function q and integrating on the domain Ω,

$$\begin{cases} \int_\Omega (-v\Delta \mathbf{u}) \cdot \mathbf{v} + \int_\Omega (\boldsymbol{u} \cdot \nabla)\boldsymbol{u} \cdot \mathbf{v} + \int_\Omega \nabla p \cdot \mathbf{v} = \mathbf{0} \\ -\int_\Omega (\nabla \cdot \mathbf{u}) \cdot \mathrm{q} = 0 \end{cases} \tag{2.6}$$

Where $\mathrm{v} \in H^1(\Omega)$ and $q \in L_0^2(\Omega)$. Although we have the nonhomogeneous boundary conditions for some region, the lifting function $l(\boldsymbol{x}) \in G$ in $H^1(\Omega)$ can be introduced to reduce the equation into the homogeneous case [30]. Applying the Divergence theorem and imposing homogeneous

boundary conditions the original problem changes into: Find $u \in G + H^1(\Omega)$ and $p \in L_0^2(\Omega)$ such that for any v $\in H_0^1(\Omega)$ and any $q \in L_0^2(\Omega)$, where

$$\begin{cases} v\int_\Omega \nabla \boldsymbol{u} \cdot \nabla \mathbf{v} + \int_\Omega (\boldsymbol{u} \cdot \nabla)\boldsymbol{u} \cdot \mathbf{v} - \int_\Omega p(\nabla \cdot \mathbf{v}) = \mathbf{0} \\ \quad -\int_\Omega (\nabla \cdot \mathbf{u}) \cdot \mathrm{q} = 0 \end{cases} \tag{2.7}$$

2.3 Space discretization

The Navier-Stokes equation, which describes the fluid flow and related fluid phenomena, is difficult to achieve the full understanding and gains a lot of attention in this area. Along with some simplified assumptions, some numerical methods are required, in order to solve for the numerical solution of Navier-Stokes equation.

After the mathematical model is selected to represent the initial problem, the space discretization method is introduced. With the appropriate discretization method in space, the differential equation in Navier-Stokes can be approximated by a system of algebraic equations at discrete location in space. In the space discretization step, we approximate the exact solution u by a finite number of values u_j at discrete nodes. Different approximation method leads to different way to represent the nodal values. In the discretization process, the appropriate polynomials with the easiness in differentiation and integration are selected to be the basis functions, which span the solution space.

In this study, finite element method is chosen for the space discretization step. In each element, the velocity is approximated by a quadratic polynomial and the pressure is approximated by a linear polynomial [30]. Thus, given the subspaces $V_h \subset H_0^1(\Omega)$ and $Q_h \subset L_0^2(\Omega)$, the equations in (2.7) changes into the following form:

$$\begin{cases} v\int_{\Omega}\ \nabla \boldsymbol{u}_h \cdot \nabla \mathbf{v}_h + \int_{\Omega}\ (\boldsymbol{u}_h \cdot \nabla)\boldsymbol{u}_h \cdot \mathbf{v}_h - \int_{\Omega}\ p(\nabla \cdot \mathbf{v}_h) = \mathbf{0} \\ -\int_{\Omega}\ (\nabla \cdot \boldsymbol{u}_h) \cdot \mathrm{q} = 0 \end{cases} \tag{2.8}$$

Where $\boldsymbol{u}_h \in V_h$ and $p_h \in Q_h$.

With the Galerkin method, we introduce two basis functions, ϕ_i for velocity and ψ_i for pressure. Then we approximate the solutions for velocity and pressure with the following formula,

$$\boldsymbol{u}_h = \sum_{j=1}^{N_u} \boldsymbol{u_j}\, \phi_i \tag{2.9}$$

$$p_h = \sum_{j=1}^{N_p}\ p_h\, \psi_i \tag{2.10}$$

Where N_u is the number of degree of freedom for velocity and N_p is the number of degree of freedom for pressure [31]. Then we substitute the linear combination of the basis functions for velocity and pressure into equation (2.8). The Galerkin formulation is shown as follow:

$$\begin{cases} v\int_{\Omega}\ \nabla \boldsymbol{u}_h \cdot \nabla \phi_i + \int_{\Omega}\ (\boldsymbol{u}_h \cdot \nabla)\boldsymbol{u}_h \cdot \phi_i - \int_{\Omega}\ p_h(\nabla \cdot \phi_i) = \mathbf{0} \\ -\int_{\Omega}\ (\nabla \cdot \boldsymbol{u}_h) \cdot \psi_i = 0 \end{cases} \tag{2.11}$$

Where for the first equation, $i = 1,2,3 \ldots, N_u$ and for the second equation, i =1,2,3 …, N_p. After the space discretization process, the system of algebraic equations is formed. The matrix form of the system is

$$\begin{cases} Au + B^T p + N(u) = \mathbf{0} \\ Bu = \mathbf{0} \end{cases} \tag{2.12}$$

Where u is the vector of unknown velocity, p is the vector of unknown pressure, Au is the discretized form of diffusion term, $N(u)$ is the discretized form of nonlinear convection, $B^T p$ is the discretized pressure term, and Bu is the discretized form of the divergence of u [30].

2.4 Linearization Scheme

In equations (2.12), the convection term is nonlinear. Thus, an appropriate linearization scheme is necessary to apply here. In this study, the Picard iteration method is utilized.

2.4.1 Picard Iteration

For the non-linear convection term $(\boldsymbol{u} \cdot \nabla)\boldsymbol{u}$, the Picard iteration utilizes the information from previous iteration to convert the non-linear term into linear form. Let k denotes the previous iteration step, and k+1 denotes the current iteration. The convection term is approximated by the following formula,

$$(u^{k+1} \cdot \nabla)u^{k+1} \approx (u^{k} \cdot \nabla)u^{k+1} \tag{2.13}$$

This approximation changes the equation (2.4) as states,

$$\begin{cases} -v\Delta \mathbf{u}^{k+1} + (\mathbf{u}^{k} \cdot \nabla)\mathbf{u}^{k+1} + \nabla \mathrm{p}^{k+1} = \mathbf{0} & in\ \Omega \\ \nabla \cdot \mathbf{u}^{k+1} = 0 & in\ \Omega \end{cases} \tag{2.14}$$

The initial guess of the solution is obtained by solving the corresponding Stokes equation. With the initial guess, u^0**,** the original Navier-Stokes equations are linearized at each iteration step [31].

2.4.2 Implemented algorithm

By solving the Stokes problem with no convection, we obtain the initial guess of u and p. Then the non-linear term N(u) in equation (2.12) is linearized by approximation in equation (2.13). By the Picard Iteration scheme, we create a linearized matrix L = $Au + N(u)$ [31]. Then the system (2.12) becomes,

$$\begin{bmatrix} L & B^T \\ B & 0 \end{bmatrix} \begin{bmatrix} u \\ p \end{bmatrix} = \begin{bmatrix} \mathbf{0} \\ \mathbf{0} \end{bmatrix} \qquad (2.15)$$

In order to help the solution converges, the relaxation parameter = 0.2 is added. This means that the new solution is composed by 20% of the previous solution and 80% of the current solution. The iteration of solving the Navier-Stokes equations terminates when the residual of the solution is less than 0.001 or the number of iteration steps reach the preset max number of iterations.

The above algorithm is implemented by FreeFem++, which is a partial differential equation solver with finite element method.

2.5 Streamline Stabilization

Although the relaxation parameter is added to the Picard iteration scheme, there is case where the solution does not converge. One way to enforce the stability of the problem is to decrease the amount of inflow. Another way to help the solution to converge is adding the streamline-diffusion term.

Considering the advantage of upwind artificial viscosity method, in this three-dimensional case, we also try to introduce the artificial diffusion term to help stabilize the initial problem. The general stabilization term is shown as

$$-Qhdiv[(\boldsymbol{b}\cdot\nabla u)\boldsymbol{b}] = -Qhdiv(\frac{\partial u}{\partial \boldsymbol{b}})\boldsymbol{b} \tag{2.16}$$

Where **b** is the transport field, and Q = $|\boldsymbol{b}|^{-1}$[32].

For case 2 to case 6, we decrease the inflow, which helps the convergence of the solutions in these cases. However, for case1, the convergence is not achieved by only reducing the inflow. Without imposing Dirichlet boundary conditions on branches, there is less restriction to impose on the problem. In this case, adding the streamline-diffusion term guarantees the convergence of solution.

Chapter 3

Results

This research followed the computational fluid dynamics procedure to investigate changes in pressure and flow split with respect to different exponents used in Murray's law. The geometry of coronary artery was generated with the data from a real patient. The 3D mesh generator, Netgen, was utilized to create the fine mesh of the given geometry. In this process, 7466 vertices and 35026 elements were generated for later simulation process. In Netgen, six regions were labeled to define the boundary conditions. We labeled wall as region 1, the inlet as region 2, the three branches as 3, 4 and 5 respectively, and finally the outlet as 6.

In this study, five cases were categorized by exponent in Murray's law and boundary conditions. Based on Murray's law and given inflow, the flow was calculated for each branch by FreeFem++ shown in Table 1, where Q_{in} denotes inflow, Q_{out} denotes outflow, Q_1, Q_2, Q_3 denote the flows in side branches respectively.

	exponent	boundary condition	Q_{in} (ml/s)	Q_1 (ml/s)	Q_2 (ml/s)	Q_3 (ml/s)	Q_{out} (ml/s)
Case 1	3.00	No	3	1.4847	0.0688	0.1585	1.2879
Case 2	3.00	Yes	3	1.4847	0.0688	0.1585	1.2879
Case 3	2.75	Yes	3	1.5744	0.0943	0.2025	1.1288
Case 4	2.5	Yes	3	1.6694	0.1291	0.2587	0.9427
Case 5	2.25	Yes	3	1.7701	0.1769	0.3306	0.7223

Table 3.1 Calculated flow for each branch based on Murray's law

The physical parameters used in the simulation were also collected from real patients. The density of the blood flow was 1.06 g/cm^3. The dynamic viscosity was 0.035 $g/cm \cdot s$. The distal pressure was 85 mmHg, which was used to set Neumann boundary condition. For the Picard iteration scheme, the Picard tolerance was set to 0.001 and the maximum number of iterations was set to 100. This means the simulation will stop either the residual is less than 0.001 or the process goes through 100 times.

With the use of FreeFem++, the numerical results of the solution were simulated with the algorithm stated in section 2.4.2. The pressure field and velocity result was generated by solving the Navier-Stokes equation with Picard iteration scheme. The computed flux at each branch was calculated by integrating the velocity on the cross-section of the vessel. The computed pressure and flux results are shown in the following tables.

	Inflow	**Branch1**	**Branch2**	**Branch3**	**Outflow**
Pressure(mmHg*1333)	742.738	0.014	1.391	0.881	0.259
Flux(ml/s**)**	2.999	-1.740	-0.086	-0.185	-0.988

Table 3.2 Pressure and flux results for case 1

	Inflow	**Branch1**	**Branch2**	**Branch3**	**Outflow**
Pressure(mmHg*1333)	114345	113755	113594	113544	113305
Flux(ml/s**)**	2.999	-1.483	-0.068	-0.157	-1.290

Table 3.3 Pressure and flux results for case 2

	Inflow	**Branch1**	**Branch2**	**Branch3**	**Outflow**
Pressure(mmHg*1333)	114189	113556	113341	113335	113305
Flux(ml/s**)**	2.999	-1.573	-0.093	-0.201	-1.132

Table 3.4 Pressure and flux results for case 3

	Inflow	Branch1	Branch2	Branch3	Outflow
Pressure(mmHg*1333)	114022	113344	113012	113071	113305
Flux(ml/s)	2.999	-1.668	-0.127	-0.257	-0.947

Table 3.5 Pressure and flux results for case 4

	Inflow	Branch1	Branch2	Branch3	Outflow
Pressure(mmHg*1333)	113847	113117	112573	112734	113305
Flux(ml/s)	2.999	-1.769	-0.174	-0.328	-0.728

Table 3.6 Pressure and flux results for case 5

The results calculated by FreeFem++ were also viewed in a visualization software, Paraview. In Figure 3.1 to Figure 3.5, the geometries with pressure field and velocity solution were shown. Red color indicated large value and blue indicated small value. The scale of the magnitude was shown in the legend.

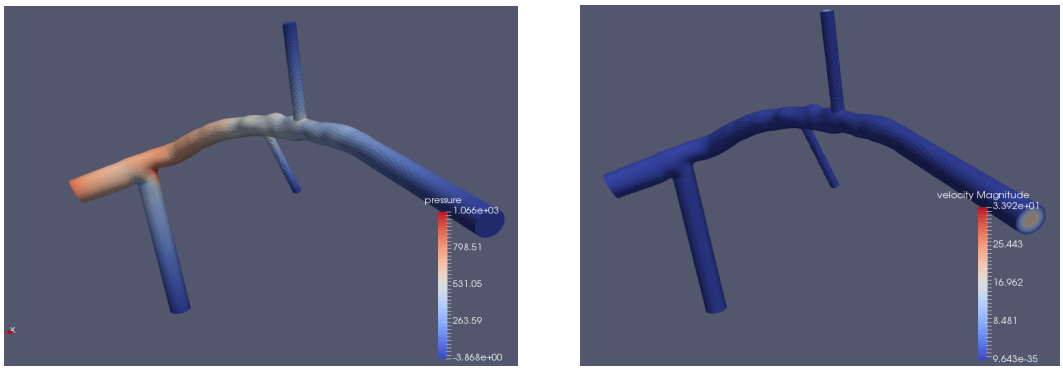

(a) Pressure (b) Velocity

Figure 3.1 The visualization of numerical results in pressure and velocity for case 1

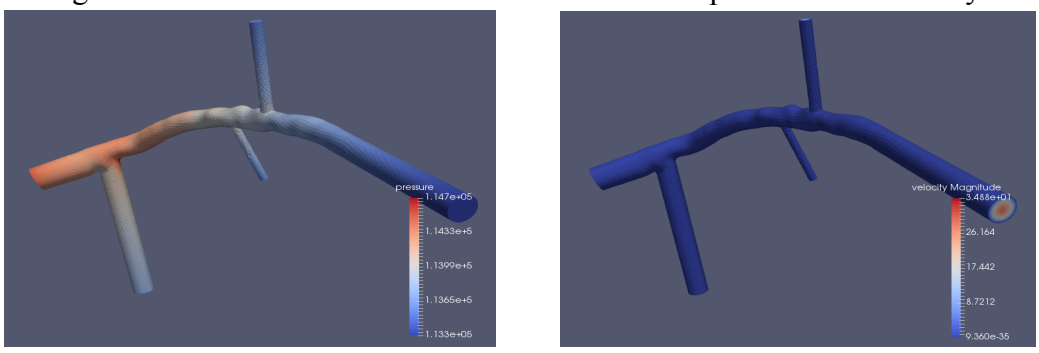

(a) Pressure (b)Velocity

Figure 3.2. The visualization of numerical results in pressure and velocity for case 2

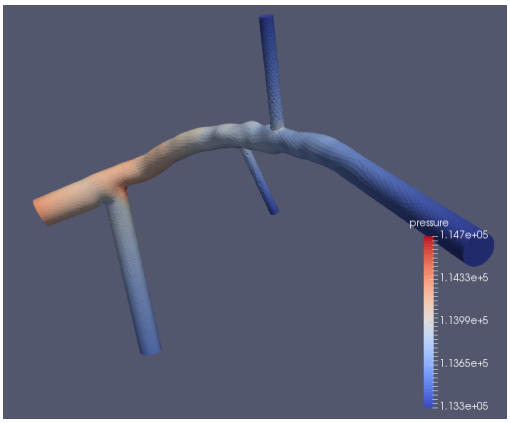

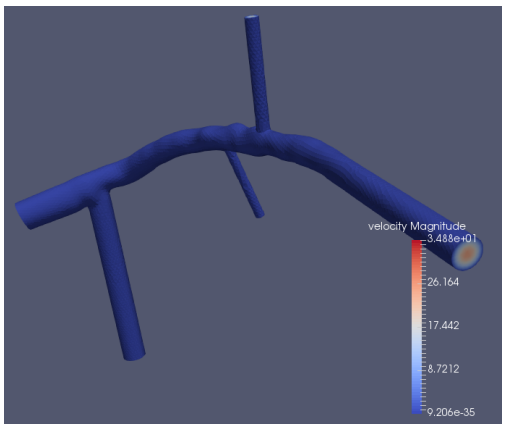

(a) Pressure (b)Velocity

Figure 3.3 The visualization of numerical results in pressure and velocity for case 3

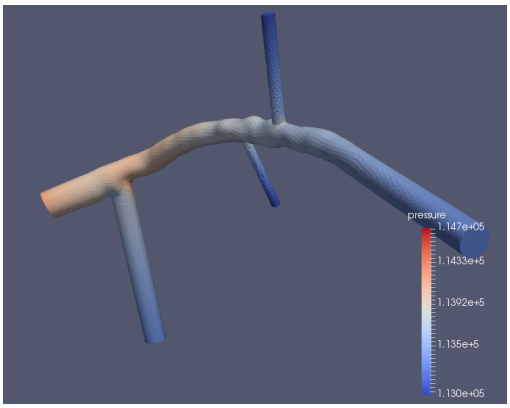

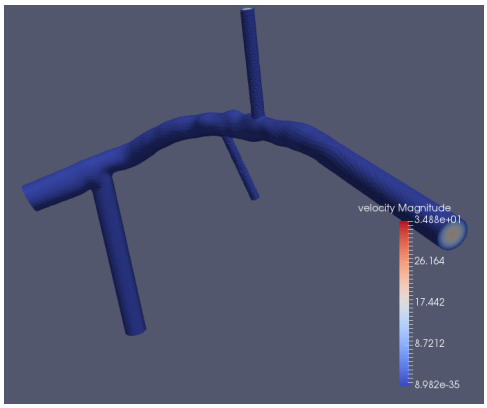

(a) Pressure (b) Velocity

Figure 3.4 The visualization of numerical results in pressure and velocity for case 4

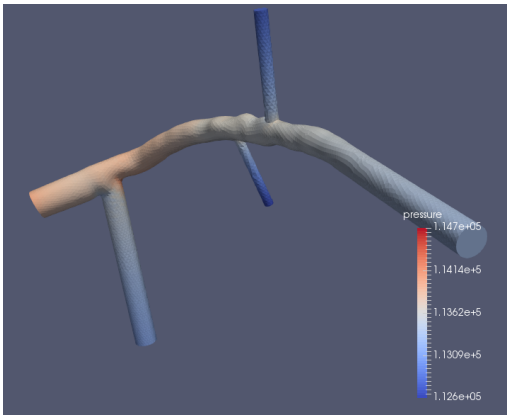

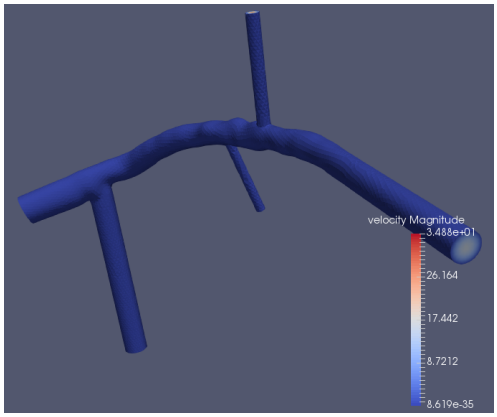

(a) Pressure (b) Velocity

Figure 3.5 The visualization of numerical results in pressure and velocity for case 5

Chapter 4

Discussion and Conclusion

In Table 3.1, the flux in each branch was calculated according to Murray's law, which was different in exponent only. With the flux data, the flow split, the ratio of outflowing flux and the inflow, was easy to obtain. We added up the flow split and compared that to 1. Because the difference between the sum of flow split and 1 was less than 0.01, the flow splitting is consistent. This indicated that every flux data we obtained has physical meaning. Such consistence allowed us to run simulations with the calculated flux information.

In Figure 3.1 to 3.5, the solutions of the Navier-Stokes equation were visualized in Paraview. We had a direct impression on the pressure and velocity changes in the given geometry. For the pressure field, the red part started from the inlet and extended to the other branches. Then the red part faded, gradually shifted to light blue, and finally became dark blue at the end of side branches and outlet in all cases. Because the color bar utilized red as the large value and blue as the small value, the pressure field solutions demonstrated the blood flow entered from the left side of the geometry and went out from the side branches and outlet. This result matched with the blood flow assumption.

The cross-section of the vessel with the velocity solution was shown in Figure 4.1. It has dense red in the center, faded to white, and gradually changed to dark blue. This indicated that the blood flow achieved its maximum velocity at the center of the vessel and had the zero velocity on the boundary. This visualization of velocity agreed with the parabolic blood profile.

To analyze the impact of changing exponent in Murray's law, we need to investigate the pressure drop and flow split results in each case. Based on the data in Table 3.2 to 3.6, the

pressure drop and flow split in side branches and outlet were determined (shown in Table 4.1 and 4.2).

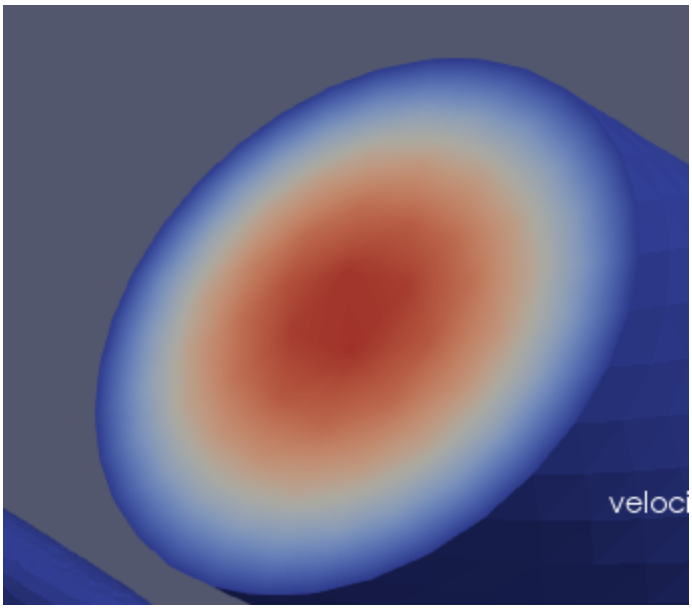

Figure 4.1 The cross-section of vessel with visualized velocity solution

Flow Split	Branch1	Branch2	Branch3	Outflow
Case1	0.5804	0.0285	0.0616	0.3295
Case2	0.4947	0.0226	0.0525	0.4302
Case3	0.5246	0.0310	0.0670	0.3775
Case4	0.5562	0.0424	0.0856	0.3157
Case5	0.5898	0.0581	0.1094	0.2427

Table 4.1 The flow split in each side branches and outflow for all five cases

Pressure Drop (mmHg)	Branch1	Branch2	Branch3	Outflow
Case1	0.5572	0.5561	0.5565	0.5570
Case2	0.4426	0.5634	0.6009	0.7802

Case3	0.4749	0.6362	0.6407	0.6632
Case4	0.5086	0.7577	0.7134	0.5379
Case5	0.5476	0.9557	0.8350	0.4066

Table 4.2 The pressure drop in each side branches and outflow for all five cases

To compare the results respect to exponent changes, we plotted the pressure drop and flow split statistics in all five cases in each branch (shown in Figure 13 and 14). First we looked at the differences in pressure drop and flow split for case 1 and case 2. Except for pressure drop in branch 2 and 3, there are relatively large change between case 1 and case 2 for all other conditions. Case 1 and case 2 share the same exponent in Murray's law, but only in case 2, boundary conditions are imposed. This shows that imposing boundary conditions on inflow and side branches will influence the pressure drop in the first side branch and outflow and flow split.in all branches.

For the data in later four cases, the monotone shift is observed. For case 2 to 5, the boundary conditions are applied, but they are different in exponent in Murray's law. Such monotone change indicates that the change of exponent in Murray's law influence the blood flow pattern. However, there is not sufficient data to investigate what kind of relationship between exponent and solution is.

To further investigate the impact of changing exponent, we plot the graphs on the same figure for pressure drop and flow split respectively (Figure 4.4 and 4.5). From Figure 4.4 and 4.5, there is less change in pressure drop and flow split for side branches and outflow from case 3 to case 4. This demonstrates that for exponents in range between 2.75 to 2.50, there is relatively less change in solution.

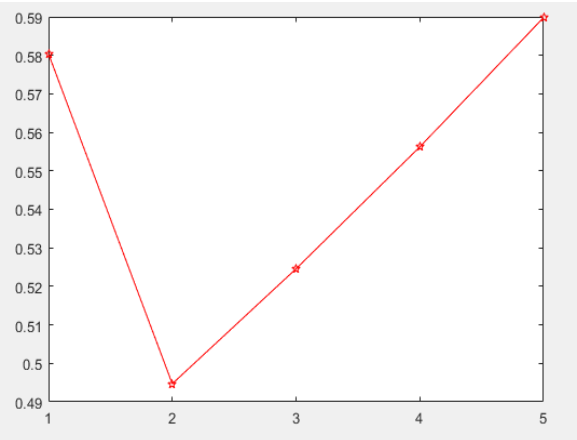

(a) Branch 1

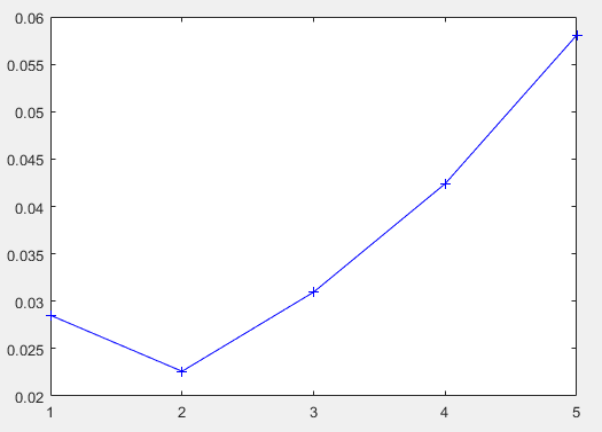

(b) Branch 2

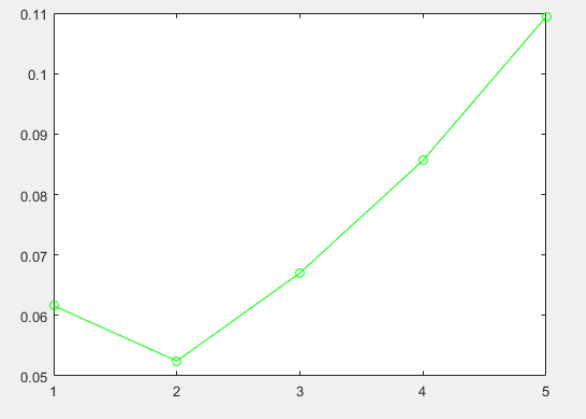

(c) Branch 3

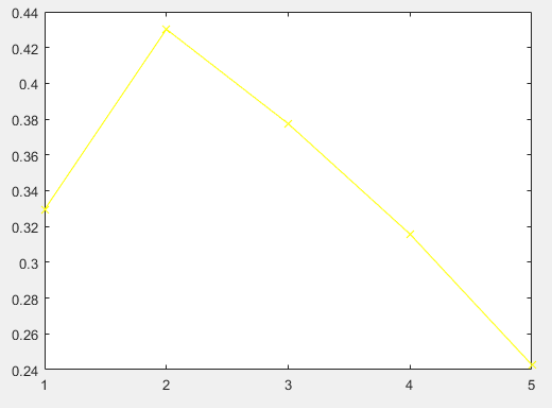

(d) Outflow

Figure 4.2 Flow split in five cases for side branches and outflow

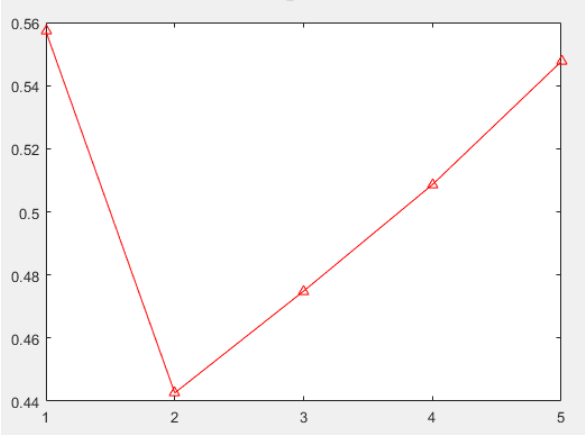

(a) Branch 1

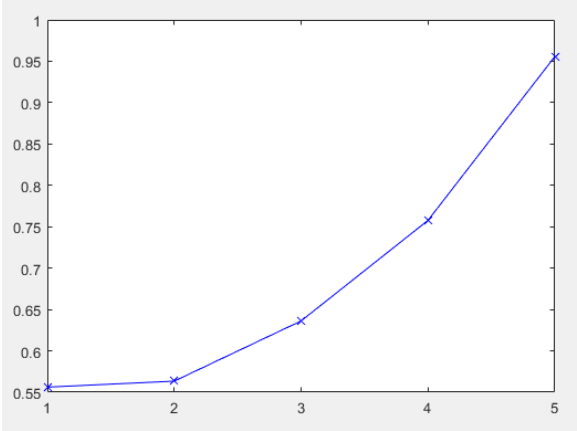

(b) Branch 2

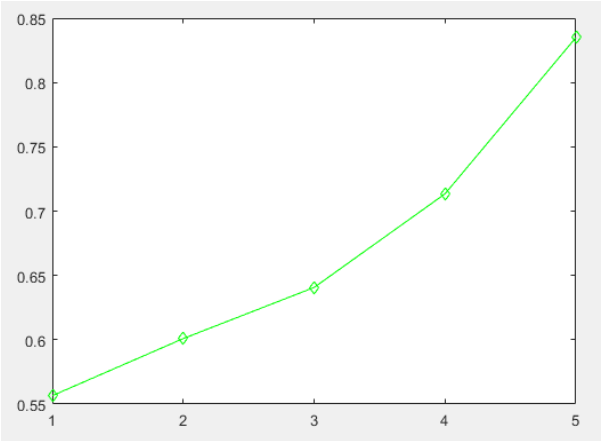

(c) Branch 3

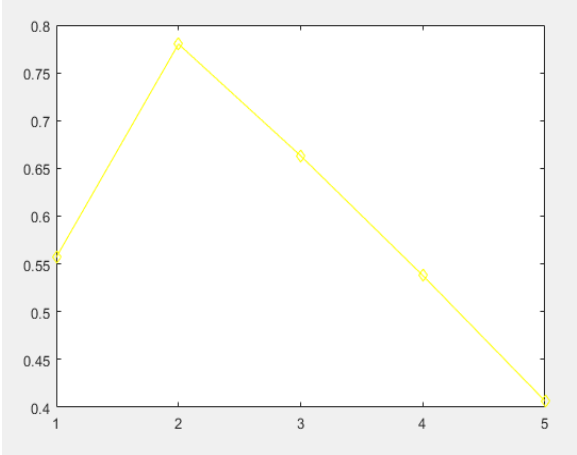

(d) Outflow

Figure 4.3 Pressure drop (mmHg) in five cases for side branches and outflow

To further investigate the impact of changing exponent, we plot the graphs on the same figure for pressure drop and flow split respectively (Figure 15 and 16). From Figure 15 and 16, there is less change in pressure drop and flow split for side branches and outflow from case 3 to case 4. This demonstrates that for exponents in range between 2.75 to 2.50, there is relatively less change in solution.

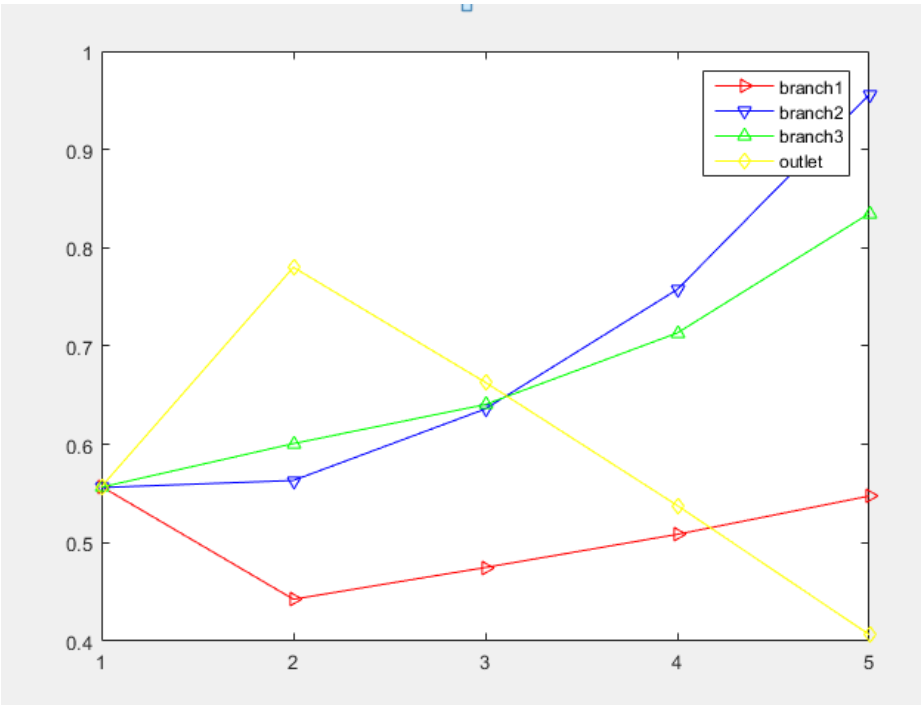

Figure 4.4 Pressure drop of five cases in side branches and outflow

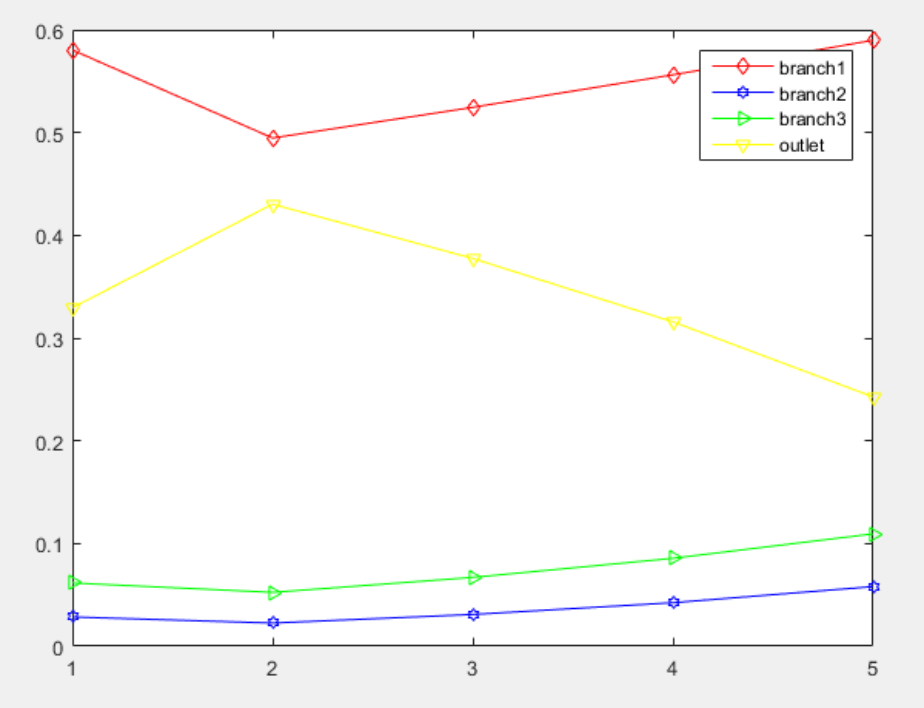

Figure 4.5 Flow split for side branches and outflow in five cases

In a conclusion, changing exponents in Murray's law has an impact on the blood flow pattern. However, the clear relation cannot be stated in this research. Choosing the exponent in range from 2.25 to 2.75 will help to reduce the sensitivity in solution resulted from the Murray's law. The results reveals the successful implement of Murray's law into real patient case and the power of CFD approach in clinical issues.

Bibliography

[1] Taber, C. W. (1941). Taber's Cyclopedic Medical Dictionary. *The American Journal of the Medical Sciences,201*(5), 771. doi:10.1097/00000441-194105000-00031

[2] "Skeletal Muscle Pump". New York Medical College. Retrieved 19 March 2013.

[3] Maton, A. (1993). *Human biology and health*. Englewood Cliffs, NJ: Prentice Hall.

[4] The Coronary Arteries - Texas Heart Institute Heart Information Center. (n.d.). Retrieved April 11, 2017, from http://www.texasheart.org/HIC/Anatomy/coroanat.cfm

[5] Ambrose, J., & Singh, M. (2015). Pathophysiology of coronary artery disease leading to acute coronary syndromes. *F1000Prime Reports,7*. doi:10.12703/p7-08

[6] Wong, N. D. (2014). Epidemiological studies of CHD and the evolution of preventive cardiology. *Nature Reviews Cardiology,11*(5), 276-289. doi:10.1038/nrcardio.2014.26

[7] Kontos, M. C., Diercks, D. B., & Kirk, J. D. (2010). Emergency Department and Office-Based Evaluation of Patients With Chest Pain. *Mayo Clinic Proceedings,85*(3), 284-299. doi:10.4065/mcp.2009.0560

[8] Bhatia, S. K. (2010). Biomaterials for Clinical Applications. doi:10.1007/978-1-4419-6920-0

[9] Mehta, P. K., Wei, J., & Wenger, N. K. (2015). Ischemic heart disease in women: A focus on risk factors. *Trends in Cardiovascular Medicine,25*(2), 140-151. doi:10.1016/j.tcm.2014.10.005

[10] Ashley EA, Niebauer J. Cardiology Explained. London: Remedica; 2004.

[11] Coronary Artery Disease. (n.d.). Retrieved April 11, 2017, from http://my.clevelandclinic.org/health/articles/coronary-artery-disease

[12] Dai, X. (2016). Genetics of coronary artery disease and myocardial infarction. *World Journal of Cardiology,8*(1), 1. doi:10.4330/wjc.v8.i1.1

[13] Ross, R. (1993). The pathogenesis of atherosclerosis: a perspective for the 1990s. *Nature,362*(6423), 801-809. doi:10.1038/362801a0

[14] Coronary Artery Disease. (n.d.). Retrieved April 11, 2017, from http://www.webmd.com/heart-disease/guide/heart-disease-coronary-artery-disease#1

[15] Chung, T. J. (2015). *Computational Fluid Dynamics*. Cambridge: Cambridge University Press.

[16] Ferziger, J. H., & Perić, M. (2012). *Computational methods for fluid dynamics*. Beijing: World Publishing Corporation.

[17] Blazek, J. (2015). *Computational fluid dynamics: principles and applications*. Butterworth-Heinemann.

[18] Gibson, C. M., Diaz, L., Kandarpa, K., Sacks, F. M., Pasternak, R. C., Sandor, T., . . . Stone, P. H. (1993). Relation of vessel wall shear stress to atherosclerosis progression in human coronary arteries. *Arteriosclerosis, Thrombosis, and Vascular Biology,13*(2), 310-315. doi:10.1161/01.atv.13.2.310

[19] Doutel, E., Pinto, S., Campos, J., & Miranda, J. (2016). Link between deviations from Murray's Law and occurrence of low wall shear stress regions in the left coronary artery. *Journal of Theoretical Biology,402*, 89-99. doi:10.1016/j.jtbi.2016.04.038

[20] Murray, C. D. (1926). The Physiological Principle of Minimum Work: I. The Vascular System and the Cost of Blood Volume. *Proceedings of the National Academy of Sciences,12*(3), 207-214. doi:10.1073/pnas.12.3.207

[21] Sherman, T. F. (1981). On connecting large vessels to small. The meaning of Murray's law. *The Journal of General Physiology,78*(4), 431-453. doi:10.1085/jgp.78.4.431

[22] Wasan, B., Cerutti, A., Ford, S., & Marsh, R. (1995). Vascular network changes in the retina with age and hypertension. *Journal of hypertension*, *13*(12), 1724-1728.

[23] Pijls, N. H., Bruyne, B. D., Peels, K., Voort, P. H., Bonnier, H. J., Bartunek, J., & Koolen, J. J. (1996). Measurement of Fractional Flow Reserve to Assess the Functional Severity of Coronary-Artery Stenoses. *New England Journal of Medicine,334*(26), 1703-1708. doi:10.1056/nejm199606273342604

[24] Brought to you by: joachimschoberl, M., M., S., U., & L. (n.d.). Netgen Mesh Generator. Retrieved April 11, 2017, from https://sourceforge.net/projects/netgen-mesher/

[25] "viscosity". Merriam-Webster Dictionary.

[26] Yurdagul, A., Finney, A. C., Woolard, M. D., & Orr, A. W. (2016). The arterial microenvironment: the where and why of atherosclerosis. *Biochemical Journal,473*(10), 1281-1295. doi:10.1042/bj20150844

[27] Chung, T. J. (2002). Computational Fluid Dynamics. doi:10.1017/cbo9780511606205

[28] Human Blood: Blood Components. (n.d.). Retrieved April 11, 2017, from http://anthro.palomar.edu/blood/blood_components.htm

[29] Bessonov, N., Sequeira, A., Simakov, S., Vassilevskii, Y., & Volpert, V. (2015). Methods of Blood Flow Modelling. *Mathematical Modelling of Natural Phenomena,11*(1), 1-25. doi:10.1051/mmnp/201611101

[30] Rehman, M. U. R. (2010). Fast iterative methods for the incompressible Navier-Stokes equations.

[31] Serur, C. E. (2013). *Fast iterative methods for solving the incompressible Navier-Stokes equations* (Doctoral dissertation, Delft University of Technology).

[32] Quarteroni, A. (2009). *Numerical models for differential problems*. Milan: Springer.